Chemical Industry & Chemical Engineering Quarterly

Available online at
Association of the Chemical Engineers of Serbia AChE
www.ache.org.rs/CICEQ

Chem. Ind. Chem. Eng. Q. 33 (1) xxx–xxx (2027) CI&CEQ

RADHAKRISHNAN MUTHUKRISHNAN[1]
https://orcid.org/0000-0001-7000-446X
PALANI GOVINDASAMY[2]
https://orcid.org/0000-0003-0909-8254
PARTHIBAN RAMACHANDRAN[3]
https://orcid.org/0009-0005-8034-5299
CHANDRASEKARAN EKAMBARAM[4]
https://orcid.org/0000-0001-9393-4184

[1]Department of Mathematics, Sri Venkateswara College of Engineering, Tamil Nadu, India
[2]Department of Mathematics, Dr.Ambedkar Govt. Arts College, Tamil Nadu, India
[3]Department of Mathematics, Nandanam Arts College, Chennai, India
[4]Department of Mathematics, Veltech Rangarajan Dr.Sagunthala R&D Institute of Science and Technology, Tamil Nadu, India

SCIENTIFIC PAPER

UDC

HEAT TRANSFER ANALYSIS OF MICRO-POLAR FLUID FLOW OVER AN EXPANDING/CONTRACTING PERMEABLE PLANE WALL

Highlights

- The governing non-linear PDEs are transformed into coupled ODEs
- The shooting technique, combined with the Runge-Kutta method, is employed for the solution
- Thermal slip conditions, thermal radiation, and non-uniform heat source/sink effects are analyzed
- A critical comparison with prior published work validates the results
- Detailed numerical solutions are obtained and examined for key physical parameters

Abstract

This research examines the stagnation-point flow of a micropolar fluid flowing past a porous, stretching or contracting flat plate, incorporating velocity and thermal slip boundary conditions. The governing partial differential equations are converted into corresponding ordinary differential equations by employing similarity transformations, which are subsequently evaluated numerically by applying a shooting technique. The influence of principal physical parameters on the distributions of velocity, microrotation, and temperature is explored and depicted through graphical representations. Furthermore, computed results for the wall shear stress coefficient and the heat transfer rate across a range of parameter values are provided in tabular format.

Keywords: boundary layer, momentum transfer, shooting technique, slip velocity, radiation, heat source/sink.

INTRODUCTION

Heat transfer over elongating and contracting surfaces has significant applications in manufacturing contexts, for instance, optical fiber manufacturing. Manufacturing elastic sheets by extrusion, metallic spinning, and the drawing of stretchable foils. The transfer of thermal energy during fluid flow across an extending plane wall with variable temperature, influenced by electric charge and internal heat generation or absorption, was investigated by Vajravelu and Rollins [1]. The viscous flow induced by a shrinking plane wall was examined by Miklavčič and Wang [2], where it was shown that the shrinking surface diverts the velocity away from the wall; hence, suitable mass suction is necessary to enhance the flow adjacent to the surface. Stagnation-point flow past a contracting plane surface was studied by Wang [3], and it was reported that the rate of heat transfer declines as the shrinking rate increases due to the growth of the boundary-layer thickness. An accurate analytical solution for flow over a shrinking plane was obtained by Fan *et al.* [4], which showed excellent agreement with numerical results using the Keller-Box method. The stagnation flow of a nanofluid over both contracting and stretching surfaces was investigated by Bachok *et al.* [5], revealing that solutions for the contracting surface are non-unique, unlike those for the stretching surface. The effect of slip boundary conditions on this problem was further analyzed by Mukhopadhyay [6], who showed that increasing the slip parameter reduces the velocity. Magnetohydrodynamic (MHD) flow past an oscillating surface, accounting for chemical reactions, thermal radiation, and viscous dissipation, was studied by Rajaraman and Muthucumaraswamy [7] using a finite-difference method. The effects of nonlinear thermal radiation on double-diffusive mixed convection stagnation-point flow of a tangent hyperbolic nanofluid subject to suction and injection conditions have been thoroughly

Correspondence: P. Govindasamy, Department of Mathematics, Dr. Ambedkar Govt. Arts College, Chennai 600039, Tamil Nadu, India.
Email: gpalani32@yahoo.co.in
Paper received: 15 August 2025
Paper revised: 17 March 2026
Paper accepted: 29 April 2026

https://doi.org/10.2298/CICEQ250815004M

examined by Kandasamy and Sivasankaran [8]. In a related study, the combined impact of activation energy and cross-diffusion on three-dimensional rotating nanofluid flow within a Darcy-Forchheimer porous medium, incorporating radiation and convective heating effects, was also investigated by Sivasankaran and Alqurashi [9]. A recent analysis by Sulochana and Nandeppanavar [10] explored the heat transfer behavior of MHD non-Newtonian fluids within a thermally stratified environment.

Many fluids, including polymeric liquids, paints, colloidal solutions, molten crystals, lubricating oils, and human blood, do not conform to Newtonian fluid theory. To address this limitation, Eringen and Math [11] introduced micropolar fluid theory, which accounts for microscopic effects arising from the micro-motions and shapes of fluid particles. In such fluids, couple stresses emerge due to microrotation. A subclass of these fluids, termed micropolar fluids, incorporates micro-spin inertia while neglecting micro-stretch effects, thereby accommodating body couples and couple stresses. This theory provides a robust framework for modeling micro-structured fluids such as polymers and rheological materials. According to Borrelli *et al.* [12], analysis was conducted on the three-dimensional micropolar fluid flow over a stationary, electrically neutral dielectric surface in equilibrium. The stagnation-point slip flow of a micropolar fluid across a porous, shrinking flat wall was examined by Parthiban *et al.* [13], who reported that suction enhances velocity, while injection increases both velocity and temperature; additionally, increasing the velocity slip parameter reduces velocity but elevates temperature. The rotating magneto-hydrodynamic flow of a micropolar fluid past a vertically oriented porous surface, incorporating thermo-diffusion (Soret effect), chemical reactions, Hall current, and ion slip, was examined by Krishna and Chamkha [14]. Also, Sharma *et al.* [15] examined how melting and slip conditions influence MHD micropolar flow of fluid over an extending surface. The influence of partial slip and cross-diffusion on MHD mixed bioconvection flow with chemical reaction has been investigated in Geetha *et al.* [16], whereas Hakeem *et al.* [17] explored magnetoconvective hybrid nanofluid slip flow past an inclined slender needle embedded in a Darcy-Forchheimer porous medium, taking viscous dissipation into account. In contrast, Madasu and Goyal [18] focused upon the creeping flow behavior of a micropolar fluid over an immiscible micropolar fluid sphere. Moreover, Abera *et al.* [19] explored the mixed convection MHD flow of a micropolar nanofluid past a stretching cylinder, incorporating the Cattaneo-Christov heat flux model and the effects of chemical reactions.

The analysis of micropolar fluids along elongating surfaces is of significant technological importance because of their extensive applications in chemical and metallurgical engineering. Rahman *et al.* [20] investigated magneto-hydrodynamic flow movement of a micropolar fluid over a nonlinearly contracting wall with variable viscosity and temperature, showing that the thermal energy transfer rate is highly influenced by the nonlinear contraction and temperature indices. The role of thermal radiation on thermal and mass transfer in the boundary layer flow of a micropolar fluid over a nonlinearly elongating surface was analyzed by Hsiao [21]. Micropolar stagnation-point flow over a flat contracting or elongating surface was examined by Yacob *et al.* [22], while Bhattacharyya *et al.* [23] studied the effect of thermal radiation on the motion of a micropolar fluid over a permeable contracting sheet. The thermal characteristics associated with stagnation-point flow past an exponentially contracting surface were reported by Bhattacharyya and Vajravelu [24]. The impact of radiative heat transfer on unsteady micropolar fluid dynamics along an elongating porous surface was demonstrated by Hussain *et al.* [25] using similarity transformations and the homotopy method. The role of chemical reactions in magnetohydrodynamic micropolar fluid flow at a stagnation point over a contracting wall was examined by Singh *et al.* [26]. Further contributions include the investigation by Kumar and Srinivas [27] into the unsteady magneto-hydrodynamic flow of an Eyring-Powell nanofluid over an inclined, permeable stretching surface, incorporating Joule heating and thermal radiation effects. In a parallel analytical study, Garg *et al.* [28] addressed micropolar fluid flow past a porous sheet while incorporating mass transpiration effects.

Fluid flow in porous media has drawn substantial interest because of its widespread occurrence in nature and its extensive applications in chemical engineering and geophysics. Fluid motion in porous channels influenced by internal heat sources or sinks plays a crucial role in many technical and manufacturing applications. Abel *et al.* [29] investigated fluid flow near a linearly contracting sheet with variable heat sources using Keller's box method. Mahmoud and Waheed [30] analyzed the influence of velocity slip on magnetohydrodynamic micropolar fluid flow past a porous contracting wall, incorporating thermal energy sources and sinks. Natural convection within a wavy porous cavity under sinusoidal thermal boundary conditions and internal heat generation was examined by Cheong *et al.* [31]. Mishra *et al.* [32] studied micropolar fluid flow across a plane wall, incorporating a source of thermal radiation, and reported that coupling and magnetic parameters significantly affect angular velocity profiles, with backflow occurring near the plate. The role of thermal radiation and cross-diffusion in unsteady chemically reactive convective flow over an extended surface embedded in a heat-generating porous medium was examined by Bhuvaneswari [33]. Additionally, Sivasankaran *et al.* [34] numerically investigated the effects of magnetic fields and discrete heating on free convection within a porous cavity. Maaitah *et al.* [35] performed a computational study of the heat characteristics of micropolar fluid flow adjacent to a vertical isothermal plate embedded within a porous medium. Palai *et al.* [36] examined the impact of uniform injection and suction on the flow behavior of a grade-three Rivlin-Ericksen fluid between porous parallel plates using a semi-analytical approach.

Motivated by prior studies, the present work investigates micropolar fluid motion near the stagnation point over an elongating plane surface, which has not been studied so far. The main objective is to analyze the stagnation-point flow behavior and thermal transfer characteristics of a micropolar fluid past an expanding/contracting permeable

plane wall. The unique contribution of this research lies in its comprehensive approach to micropolar fluid flow, incorporating thermal slip boundary conditions, thermal radiation, along with a spatially varying heat source/sink acting simultaneously. To the best of the authors' knowledge, the combined influence of these effects on heat transfer characteristics, microrotation distribution, the coefficient of skin friction, and Nusselt number for such a configuration has not been reported in the literature. The coupling of wall expansion/contraction with permeability and micropolar microstructural effects introduces new physical interactions that significantly alter the boundary-layer structure. Furthermore, the existence of dual solutions for contracting surfaces is examined, and a stability analysis is conducted to identify the physically realizable solution branches-an aspect that has received limited attention in previous studies.

The results offer an important understanding of the thermal characteristics of micropolar fluids in the presence of surface stretching/shrinking, radiation, slip conditions, and spatial heat generation/absorption, with relevance to modern engineering applications. Future investigations may extend the present model to include nonlinear radiation, temperature-dependent properties, magneto-hydrodynamic effects, viscous dissipation, nonlinear slip, unsteady or three-dimensional flows, and entropy generation, supported by experimental or direct numerical simulation (DNS) validation.

MODELLING EQUATIONS

We examine a two-dimensional stagnation-point flow involving a micropolar fluid. This flow occurs along a flat, porous surface that stretches linearly and is influenced by conditions of velocity slip. The corresponding flow geometry is shown in Figure 1.

The velocities at the surface and in the free stream are taken to be $\hat{u}_w(\hat{x}) = a\hat{x}$ and $\hat{u}_e(\hat{x}) = c\hat{x}$, respectively. The wall temperature is prescribed as $\hat{T}_w(\hat{x}) = \hat{T}_\infty + b\hat{x}$ where $a > 0,\ b > 0$ and $c > 0$ and $\hat{T}_\infty$ denotes the free-stream temperature. The $\hat{x}$ - axis is aligned with the surface of the plane. The effects of microstructural interactions and viscous diffusion are assumed to be negligible, leading to a reduction of the total spin $\hat{N}$ attributed solely to microrotation.

Under these assumptions, the governing equations are presented below:

$$\frac{\partial \hat{u}}{\partial \hat{x}} + \frac{\partial \hat{v}}{\partial \hat{y}} = 0 \qquad (1)$$

$$\hat{u}\frac{\partial \hat{u}}{\partial \hat{x}} + \hat{v}\frac{\partial \hat{u}}{\partial \hat{y}} = \hat{u}_e\frac{\partial \hat{u}_e}{\partial \hat{x}} + \frac{\mu}{\rho}\frac{\partial^2 \hat{u}}{\partial \hat{y}^2} + \frac{\kappa}{\rho}\left[\frac{\partial^2 \hat{u}}{\partial \hat{y}^2} + \frac{\partial \hat{N}}{\partial \hat{y}}\right] \qquad (2)$$

$$\rho j\left[\hat{u}\frac{\partial \hat{N}}{\partial \hat{x}} + \hat{v}\frac{\partial \hat{N}}{\partial \hat{y}}\right] = \gamma\frac{\partial^2 \hat{N}}{\partial \hat{y}^2} - \kappa\left[2\hat{N} + \frac{\partial \hat{u}}{\partial \hat{y}}\right] \qquad (3)$$

$$\hat{u}\frac{\partial \hat{T}}{\partial \hat{x}} + \hat{v}\frac{\partial \hat{T}}{\partial \hat{y}} = \frac{\kappa}{\rho C_p}\frac{\partial^2 \hat{T}}{\partial \hat{y}^2} - \frac{1}{\rho C_p}\frac{\partial q_r}{\partial \hat{y}} + \frac{Q_0}{\rho C_p}\left[\hat{T} - \hat{T}_\infty\right] \qquad (4)$$

$$\gamma = \left[\mu + \frac{\kappa}{2}\right] l = \mu\left[\mu + \frac{\Delta}{2}\right] l \qquad (5)$$

where $\hat{u}$ and $\hat{v}$ are the dimensional velocities along and normal to the surface respectively, $\hat{x}$ and $\hat{y}$ represent the direction along and normal to the surface, μ is the fluid viscosity, ρ is the density of the fluid, κ is the rotational viscosity, $\hat{N}$ is the microrotation component, j is the density of micro inertia, γ is the rotational gradient, C_p is the specific heat at constant pressure, Q_0 is the volumetric thermal source/sink, μ is the fluid viscosity, l is the representative length, and Δ is the micropolar coefficient.

In the Roseland approximation, radiative heat transfer is described by the equation:

$$q_r = \frac{4\sigma^*}{3k^*}\frac{\partial \hat{T}^4}{\partial \hat{y}} \qquad (6)$$

where σ^* stands for the Stefan-Boltzmann constant, k^* denotes the average absorption coefficient.

Taking the stream's local temperature allows $\hat{T}^4$ to be represented as a Taylor expansion around $\hat{T}_\infty$, and disregarding terms of higher order, one obtains $\hat{T}^4 = 4\hat{T}_\infty^3\hat{T} - 3\hat{T}_\infty^4$.

Consequently, Eq. (4) may be represented as:

$$\hat{u}\frac{\partial \hat{T}}{\partial \hat{x}} + \hat{v}\frac{\partial \hat{T}}{\partial \hat{y}} = \frac{\kappa}{\rho C_p}\frac{\partial^2 \hat{T}}{\partial \hat{y}^2} + \frac{16\sigma^*\hat{T}_\infty^3}{3\rho C_p k^*}\frac{\partial^2 \hat{T}}{\partial \hat{y}^2} + \frac{Q_0}{\rho C_p}\left[\hat{T} - \hat{T}_\infty\right] \qquad (7)$$

Associated boundary parameters:

$$\hat{u} = \hat{u}_w(\hat{x}) = A\frac{\partial \hat{u}}{\partial \hat{y}} + a\hat{x}$$

$$\hat{v} = \hat{v}_w(\hat{x})$$

$$\hat{N} = -n\frac{\partial}{\partial \hat{y}}(\hat{u})$$

$$\hat{T} = \hat{T}_W(\hat{x}) = B\frac{\partial \hat{T}}{\partial \hat{y}} + \hat{T}_\infty \ \ at\ \ \hat{y} = 0 \qquad (8)$$

$$\hat{u} = \hat{u}_e(\hat{x}) = c\hat{x}$$

$$\hat{N} \to 0$$

$$\hat{T} \to \hat{T}_\infty \text{ as } \hat{y} \to \infty \qquad (9)$$

where $\hat{v}_w(\hat{x})$ is the transpiring surface velocity and $n(0 \le n \le 1)$ is the boundary measure for the vortex state. Here, $n = 0,\ i.e.,\ \widehat{N} = 0,$ indicates the non-vortex condition, that is, the micro particles in the dense flow are not able to rotate close to the wall, and $n = \frac{1}{2}$ signifies the asymmetric portion of the stress tensor disappearing, which means fluid dilution near the wall. Also, $n = 1$ reveals the turbulent flows. Here $\hat{v}_w(\hat{x}) < 0$ means mass suction and $\hat{v}_w(\hat{x}) > 0$ means mass injection.

The transformations ensuring similarity, as listed below, are introduced:

$$\eta = \sqrt{\frac{c}{\nu}}\hat{y}$$

$$\psi = \sqrt{c\nu}\hat{x}\, f(\eta)$$

$$\widehat{N} = \left(c\hat{x}\sqrt{\frac{c}{\nu}}\, g(\eta)\right)$$

$$\theta = \frac{\hat{T} - \hat{T}_\infty}{\hat{T}_W - \hat{T}_\infty} \qquad (10)$$

where η is the resemblance variable, ψ is the stream function operation satisfying $\hat{u} = \frac{\partial \psi}{\partial \hat{y}}$, $\hat{v} = -\frac{\partial \psi}{\partial \hat{x}}$ and Eq. (1).

The modelling Eqs. (2) and (4) become ODEs:

$$[1 + \Delta]\mathrm{f}''' + \mathrm{ff}'' - \mathrm{f}'^2 + \Delta\mathrm{g}' + 1 = 0 \qquad (11)$$

$$\left[1 + \frac{\Delta}{2}\right]\mathrm{g}'' + \mathrm{fg}' - \mathrm{f}'\mathrm{g} - 2\Delta\mathrm{g} - \Delta\mathrm{f}'' = 0 \qquad (12)$$

$$[1+\mathrm{R}]\theta'' - \mathrm{Pr}[\mathrm{f}'\theta - \mathrm{f}\theta'] + \mathrm{PrQ}\theta = 0 \qquad (13)$$

with the boundary settings Eqs. (7) and (8) becoming:

$$\mathrm{f}(0) = \mathrm{s}$$
$$\mathrm{f}'(0) = \epsilon + \lambda \mathrm{f}''(0)$$
$$\frac{1}{\mathrm{n}}\mathrm{g}(0) = -\mathrm{f}''(0)$$
$$\theta(0) = \delta\theta'(0) + 1 \qquad (14)$$
$$\mathrm{f}'(\infty) = 1$$
$$\mathrm{g}(\infty) = 0$$
$$\theta(\infty) = 0 \qquad (15)$$

where f'- is the non-dimensional velocity of the fluid, g'- non-dimensional form of angular velocity, θ - is the non-dimensional temperature, $s = -\frac{\hat{v}_w}{\sqrt{cv}}$ - is the suction/injection value; $R = \frac{16\sigma^* T_\infty^3}{3kk^*}$ - is the radiation parameter; $\mathrm{Pr} = \frac{\mu C_p}{k}$ - is the Prandtl number; $Q = \frac{Q_0}{c\rho C_p}$ - is the heat source/sink; $\epsilon = \frac{a}{c}$ - is the stretching factor; $\lambda = A\sqrt{\frac{c}{\nu}}$ is the velocity slip factor; and $\delta = B\sqrt{\frac{c}{\nu}}$ is the thermal slip factor.

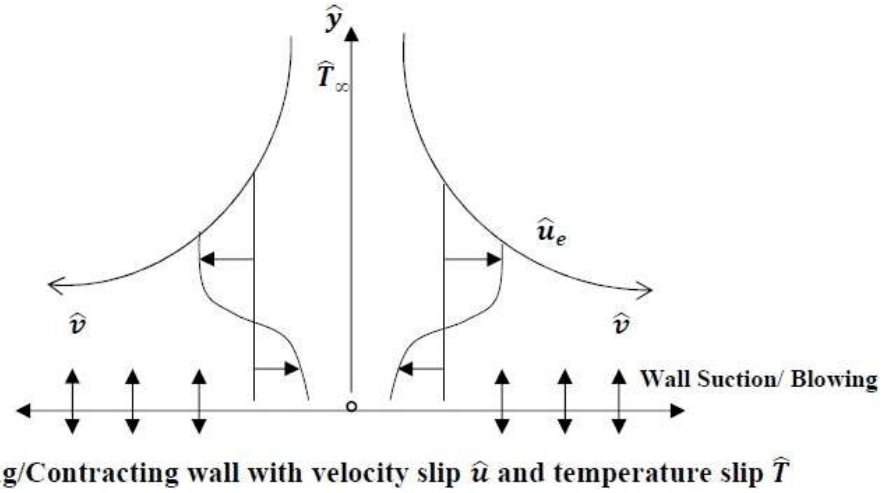

Figure 1. Physical Model.

The physical features, like the shear stress C_f, the couple stress $M_{\hat{x}}$, and the Nusselt number $\mathrm{N\hat{u}}_{\hat{x}}$, are defined as follows:

$$C_f = \frac{\tau_w}{\rho \hat{u}_e^2}$$
$$M_{\hat{x}} = \frac{m_w}{\rho v \hat{u}_e}$$
$$\mathrm{N\hat{u}}_{\hat{x}} = \frac{\hat{x} q_w}{k(\hat{\mathrm{T}}_\mathrm{w} - \hat{\mathrm{T}}_\infty)} \qquad (16)$$

where the plane shear stress τ_w, the plane couple stress m_w, and the plane's heat q_w are given by:

$$\tau_w = \left[(\mu + \kappa)\frac{\partial \hat{u}}{\partial \hat{y}} + \kappa \hat{N}\right]_{\hat{y}=0}$$
$$m_w = \left[\left(\mu + \frac{\kappa}{2}\right) l \frac{\partial \hat{N}}{\partial \hat{y}}\right]_{\hat{y}=0}$$
$$q_w = -\left(\kappa + \frac{16\ {}^*\hat{T}_\infty^3}{3k^*}\right)\left(\frac{\partial \hat{T}}{\partial \hat{y}}\right)_{\hat{y}=0} \qquad (17)$$

Using Eq. (16), the following expression is obtained:

$$\mathrm{Re}_{\hat{x}}^{1/2} C_f = [1 + \Delta - \Delta n] f''(0)$$
$$M_{\hat{x}} = \left(\frac{2+\Delta}{2}\right) g'(0)$$
$$\mathrm{Re}_{\hat{x}}^{-1/2} \mathrm{N\hat{u}}_{\hat{x}} = -(1+R)\theta'(0) \qquad (18)$$

where $\mathrm{Re}_{\hat{x}} = \frac{1}{v}[\hat{u}_e(\hat{x})\hat{x}]$ is the local Reynolds number.

NUMERICAL PROCEDURE

Using the shooting method, Eqs. (11), (12), and (13), under the given boundary conditions prescribed in Eqs. (14) and (15), are expressed in the form of a first-order differential system.

$$p = \mathrm{f}'$$
$$q = p'$$
$$q' = [1 + (1+\Delta)][-\mathrm{f}q + p^2 - \Delta h - 1] \qquad (19)$$
$$\mathrm{g}' = h$$
$$h' = [1/(1 + (\Delta/2))][-\mathrm{f}h + pg + \Delta(2g + q] \qquad (20)$$
$$\theta' = z$$
$$z' = [1/(1+\mathrm{R})][\mathrm{Pr}(\theta p - \mathrm{f}z) - \mathrm{PrQ}\theta] \qquad (21)$$

and the boundary setting:

$$f(0) = \mathrm{s}$$
$$p(0) = \epsilon + \lambda q(0)$$
$$g(0) = -\eta q(0)$$
$$\theta(0) = 1 + \delta z(0) \qquad (22)$$

To solve the system of Eqs. (19) to (21) of the seven first-order ODEs as an IVP, we need seven initial settings $f(0)$, $p(0)$, $q(0)$, $g(0)$, $h(0)$, $\theta(0)$ *and* $z(0)$, which are all available with the availability of the unknown four initial values $q(0)$, $h(0)$ and $z(0)$, i.e., $f''(0)$, $g'(0)$, and $\theta'(0)$.

Therefore, the preliminary values for $f''(0)$, $g'(0)$, and $\theta'(0)$ are assumed to compute the above system numerically. To guarantee the convergence, we choose a suitable fixed value η_∞ representing $\eta\to\infty$. The evaluated outcomes for $f'(0)$, $g(0)$ and $\theta(0)$ at η_∞ are matched with the expected values at $\eta = \eta_\infty$. To improve the precision of the computed solution, the estimated results of $f''(0)$, $g'(0)$, and $\theta'(0)$ are modified, and the process continues until the desired outcomes are attained.

FINDINGS AND EXAMINATIONS

The velocity, angular velocity, and temperature are computed numerically for varying data of s and Δ, while keeping other parameters constant. Positive values of s indicate suction at the plate, whereas values below zero represent injection. The current values of $f''(0)$ and $-\theta'(0)$ are evaluated against the findings reported elsewhere [3,22,26], as presented in Table 1. The current results show strong consistency with previously reported findings.

Figure 2(a) illustrates that increasing the micropolar parameter (Δ) results in a decrease in the fluid velocity. Physically, this means the fluid's microstructure resists flow more efficiently, enhancing the fluid's apparent viscosity and dropping velocity. Furthermore, higher values Δ result in a thicker boundary layer, indicating that more micro-elements accumulate near the surface. Physically, this means the improved rotational viscosity and increased resistance to flow permit micro-elements to concentrate near the surface, thickening the boundary layer and reducing fluid velocity. As presented in Figure 2(b), the fluid velocity is generally higher under suction conditions compared to injection. Under suction, the velocity gradually increases with η, which promotes the development of the boundary layer. Figure 2(c) demonstrates that the velocity is lower for the shrinking surface, whereas it increases with the velocity ratio parameter $\epsilon = a/c$ for the stretching surface. Notably, when $\epsilon = a/c < 1$, the free-stream velocity increases; otherwise, the elongating surface velocity rises. In both cases, the velocity profile exhibits an overall increase. Figure 2(d) indicates that increasing the velocity slip, λ, enhances the velocity profile, as a higher slip reduces the frictional resistance between the viscous fluid and the surface.

Figure 3(a) shows that an enhancement in the thermal slip parameter δ results in a decline in the boundary-layer temperature, which can be attributed to the weakening of convective heat transfer within the thermal boundary layer. Figures 3(b)-3(d) indicate that higher values of the heat source parameter (Q) and the radiation parameter (R) enhance the temperature distribution in the boundary layer for $\epsilon = a/c < 1$, whereas increasing the Prandtl number (Pr) leads to a reduction in fluid temperature. This means that increased internal heat generation within the fluid raises the temperature of the fluid. Further energy absorption increased by enhanced radiative heat transfer, resulting in boosting the fluid's temperature.

Figure 4(a) illustrates that the micropolar factor (Δ) enhances angular momentum in the region near the sheet, while its effect diminishes with increasing distance. In Figure 4(b), it is evident that angular velocity decreases for a shrinking surface but increases with the velocity ratio parameter ($\epsilon = a/c$) for a stretching surface. Figure 4(c) indicates that the suction parameter (s) reduces angular momentum near the surface; however, this effect reverses at locations farther from the surface. Finally, Figure 4(d) demonstrates that increasing the velocity slip parameter (λ) enhances the angular velocity. Increasing the velocity slip parameter (λ), reducing the frictional resistance at the surface, allows the fluid to slip and enhance the angular velocity of micro-elements near the surface.

Table 2 illustrates the influence of the parameters Δ, ϵ, s, Q, R, λ, δ, and Pr on $f''(0)$ (shear stress) and $-\theta'(0)$ (temperature gradient). A negative wall heat flux indicates that thermal energy passes from the surface into the fluid layer adjacent to it. A negative wall heat flux indicates heat transfer from the surface to the fluid, which increases the temperature of the fluid near the surface. The numerical results show that increasing Δ, ϵ, and λ leads to a reduction in shear stress, whereas an increase in s produces the opposite effect. Furthermore, the shear stress remains essentially unchanged with variations in Q, R, δ, λ, and Pr. In contrast, the temperature gradient increases with increasing ϵ, s, λ, and Pr, while higher values of Δ, Q, R, and δ result in a decrease in the temperature gradient.

Table 1. Comparison outcomes for different parameter values of ϵ, Δ, n=0.5, Pr=1.0 and s= δ=Q=0.

∈	Δ	[2]	[22]		[26]		Our Result	
		$f''(0)$	$f''(0)$	$-\theta'(0)$	$f''(0)$	$-\theta'(0)$	$f''(0)$	$-\theta'(0)$
0	0	1.2326	1.2326	-0.5705	1.2326	-0.5705	1.2326	-0.5705
0	1	-	1.0064	-0.5445	1.0064	-0.5445	1.0064	-0.5445
0.5	0	0.7133	0.7133	-0.6921	0.7133	-0.6921	0.7135	-0.6921

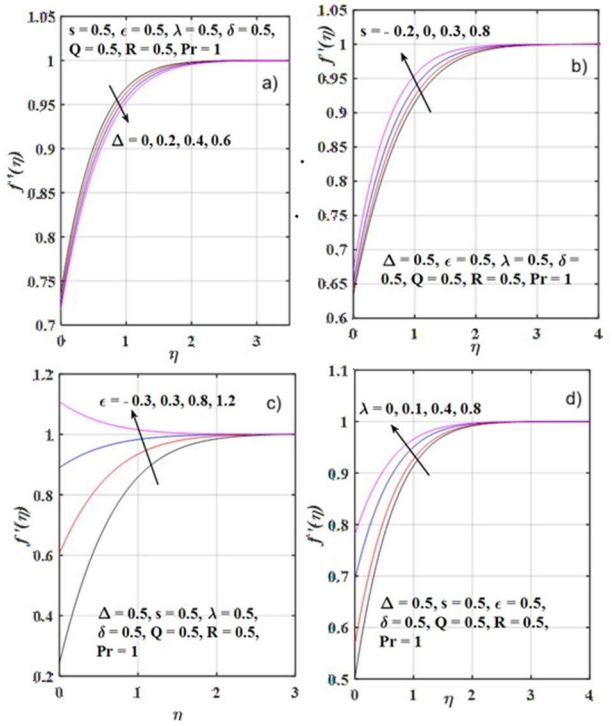

Figure 2. a) Outcome for Δ in terms of $f'(\eta)$ b) Outcome for s in terms of $f'(\eta)$ c) Outcome for ϵ in terms of $f'(\eta)$ d) Outcome for λ in terms of $f'(\eta)$.

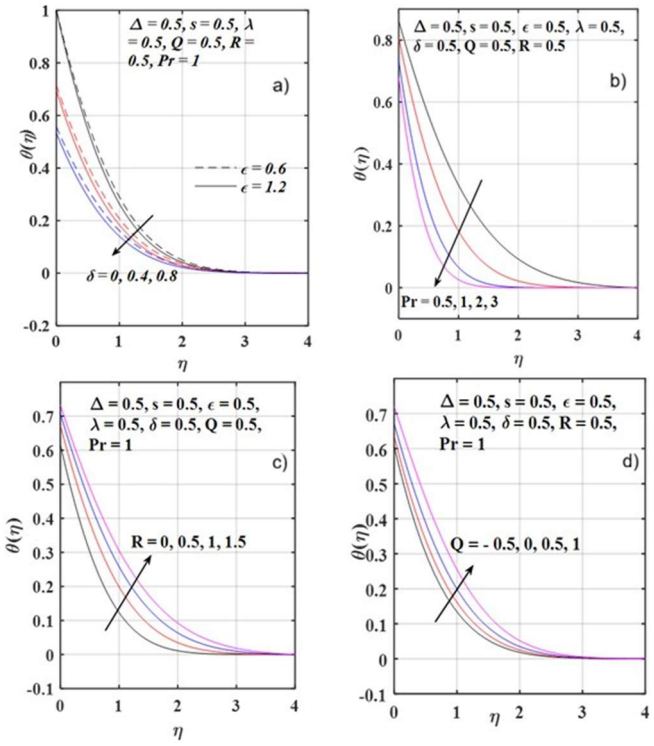

Figure 3. a) Outcome for δ in terms of $\theta(\eta)$ b) Outcome for Pr in terms of $\theta(\eta)$ c) Outcome for R in terms of $\theta(\eta)$ d) Outcome for Q in terms of $\theta(\eta)$.

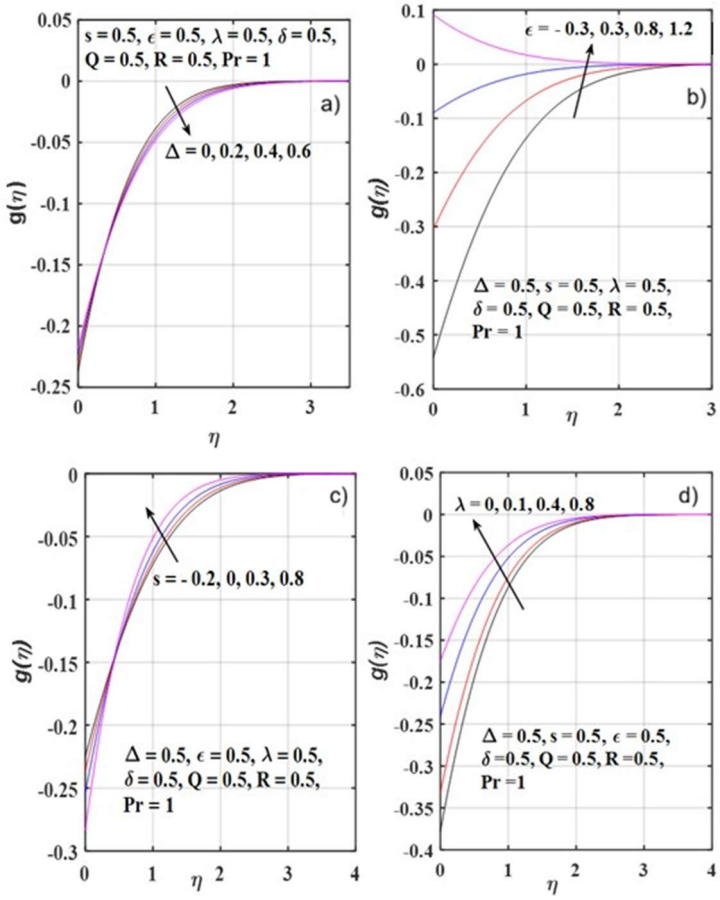

Figure 4. a) Outcome for Δ in terms of $g(\eta)$ b) Outcome for ϵ in terms of $g(\eta)$ c) Outcome for s in terms of $g(\eta)$ d) Outcome for λ in terms of $g(\eta)$.

Table 2. The variance of $f''(0), -\theta'(0)$is presented for the grouped parameter values at $n = 0.0$

S. No	Δ	ϵ	s	Q	R	λ	δ	Pr	$f''(0)$	$-\theta'(0)$
1	**0.5**	0.5	0.5	0.5	0.5	0.5	0.5	1	0.4412	0.6555
2	**1**	0.5	0.5	0.5	0.5	0.5	0.5	1	0.4150	0.6512
3	**1.5**	0.5	0.5	0.5	0.5	0.5	0.5	1	0.3933	0.6474
4	0.5	**-0.5**	0.5	0.5	0.5	0.5	0.5	1	1.7749	0.6431
5	0.5	**0.5**	0.5	0.5	0.5	0.5	0.5	1	0.4412	0.6555
6	0.5	**1.2**	0.5	0.5	0.5	0.5	0.5	1	- 0.1831	0.7089
7	0.5	0.5	**0**	0.5	0.5	0.5	0.5	1	0.4010	0.5461
8	0.5	0.5	**0.5**	0.5	0.5	0.5	0.5	1	0.4412	0.6555
9	0.5	0.5	**0.8**	0.5	0.5	0.5	0.5	1	0.4646	0.7181
10	0.5	0.5	0.5	**-0.5**	0.5	0.5	0.5	1	0.4412	0.7850
11	0.5	0.5	0.5	**0**	0.5	0	0.5	1	0.4412	0.7277
12	0.5	0.5	0.5	**0.5**	0.5	0.5	0.5	1	0.4412	0.6555
13	0.5	0.5	0.5	0.5	**0**	0.5	0	1	0.4412	0.7672
14	0.5	0.5	0.5	0.5	**0.5**	0.5	0.5	1	0.4412	0.6555
15	0.5	0.5	0.5	0.5	**1**	0.5	1	1	0.4412	0.5842
16	0.5	0.5	0.5	0.5	0.5	**0**	0.5	1	0.7565	0.6200
17	0.5	0.5	0.5	0.5	0.5	**0.4**	0.5	1	0.4824	0.6513
18	0.5	0.5	0.5	0.5	0.5	**0.8**	0.5	1	0.3506	0.6644
19	0.5	0.5	0.5	0.5	0.5	0.5	**0**	1	0.4412	0.9750
20	0.5	0.5	0.5	0.5	0.5	0.5	**0.4**	1	0.4412	0.7015
21	0.5	0.5	0.5	0.5	0.5	0.5	**0.8**	1	0.4412	0.5478
22	0.5	0.5	0.5	0.5	0.5	0.5	0.5	**0.5**	0.4412	0.4958
23	0.5	0.5	0.5	0.5	0.5	0.5	0.5	**1**	0.4412	0.6555
24	0.5	0.5	0.5	0.5	0.5	0.5	0.5	**2**	0.4412	0.8538

CONCLUSION

The significance of Δ, ϵ, s, Q, R, λ, δ, and Pr on $f'(0)$, $g(0)$ and $\theta(0)$ are summarized as follows. The micropolar parameter Δ diminishes the velocity distribution along the boundary layer but increases the temperature there. However, an opposite trend is observed with respect to the parameters ϵ, s, and λ. The thermal slip δ decreases the temperature but does not change the velocity. The parameters Q and R increase the temperature profile, and temperatures are larger in the suction case than in the injection case. The parameter Pr does not influence the velocity but decreases the temperature trace. The shearing stress $f''(0)$ is constant for the parameters Q, R, Pr, δ, but increases for s and λ. The temperature gradient $-\theta'(0)$ decreases for the parameters Q, R, λ, and δ but increases for ϵ, s, and Pr.

Such a study is found useful in the field of industrial coatings and films, membrane separation processes, chemical reactor design, enhanced oil recovery, thermal management in process equipment, crystal growth processes, electrochemical processes, catalytic reactions, pharmaceuticals, colloidal chemistry, biomedical, and environmental engineering.

NOMENCLATURE:

n Boundary value coefficient

h_f Coefficient of heat transfer$[Wm^{-2}K^{-1}]$

a Denote the wall expansion coefficient

j Density of micro inertia$[Kgm^{-1}]$

$\hat{x}$ Direction along the surface

$\hat{y}$ In the direction normal to the surface

L Length

$\hat{N}$ Micro-rotation component

g' Non-dimensional form of angular velocity

$\hat{v}$ Normal velocity at the surface [m/s]

$l = \frac{\vartheta}{c}$ Representative length$[m]$

C_p Represents the specific heat at constant pressure

c The free stream flow rate coefficient

f' The non-dimensional velocity of the fluid

$\hat{u}$ Velocity at the surface$[ms^{-1}]$

Q_0 Volumetric thermal source/sink

Greek Symbols:

η Boundary layer length

ρ Density of the fluid$[Kgm^{-3}]$

μ Fluid viscosity$[Pa.s]$

Δ Micropolar coefficient

ν Momentum diffusivity$[m^2s^{-1}]$

θ Non-dimensional temperature

γ Rotational gradient

κ Rotational viscosity$[Pa.s]$

REFERENCES

[1] K. Vajravelu, D. Rollins, Int. J. Non-Linear Mech.27 (1992) 265-277. https://doi.org/10.1016/0020-7462(92)90085-L.

[2] M. Miklavčič, C. Y. Wang, Q. Appl. Math. 64(2006) 283-290. http://www.jstor.org/stable/43638726.

[3] C.Y. Wang, Int. J. Non-Linear Mech. 43 (2008) 377-382. https://doi.org/10.1016/j.ijnonlinmec.2007.12.021

[4] T. Fan, Hang Xu, I. Pop, Int. Commun. Heat Mass Transf. 37 (2010) 1440-1446. https://doi.org/10.1016/j.icheatmasstransfer.2010.08.002.

[5] N. Bachok, A. Ishak, I. Pop, ASME J. Heat Transfer, 135 (2013) 054501. https://doi.org/10.1115/1.4023303.

[6] S. Mukhopadhyay, Alexandria Eng. J.52 (2013) 563-569. https://doi.org/10.1016/j.aej.2013.07.004.

[7] R. Rajaraman, R. Muthucumaraswamy, Chem. Ind. Chem. Eng. Q. 30 (2024) 223-230. https://doi.org/10.2298/CICEQ230526025R.

[8] J. Kandasamy, S. Sivasankaran, Aircr. Eng. Aerosp. Technol. 97(2025) 514-521. https://doi.org/10.1108/AEAT-05-2024-0131.

[9] S. Sivasankaran, J. Alqurashi, Open Phys., 23(2025) 1-14. https://doi.org/10.1515/phys-2025-0186.

[10] C. Sulochana, A.L. Nandeppanavar, J. Res. Appl. Mech. Eng. 13 (2025) 1-23. https://ph01.tci-thaijo.org/index.php/jrame/article/view/255478.

[11] A.C. Eringen, J. Math. Mech. 16 (1966) 1-18. http://www.jstor.org/stable/24901466.

[12] A. Borrelli, G. Giantesio, M.C. Patria, Commun. Nonlinear Sci. Numer. Simul. 20 (2015) 121-135. https://doi.org/10.1016/j.cnsns.2014.04.011.

[13] R. Parthiban, G. Palani, S. Tinker, R. P. Sharma, Int. J. Appl. Mech. Eng. 26 (2021) 173-85. https://doi.org/10.2478/ijame-2021-0026.

[14] M.V. Krishna, A.J. Chamkha, Int. J. Ambient Energy. 43(2021)5344-5356. https://doi.org/10.1080/01430750.2021.1946146.

[15] S. Sharma, A. Dadheech, A. Parmar, J. Arora, Q. Al-Mdallal, S. Saranya, Sci. Rep.13 (2023) 10715. https://doi.org/10.1038/s41598-023-36988-3.

[16] S. P. Geetha, S. Sivasankaran, M. Bhuvaneswari, J. Nanofluids, 12(2023) 1815-1826. https://doi.org/10.1166/jon.2023.2063.

[17] A. Hakeem, G. Bhose, S. Sivasankaran, Int. J. Numer. Methods Heat Fluid Flow, 34(2024) 334-352. https://doi.org/10.1108/HFF-04-2023-0200.

[18] K. Madasu, N. Goyal, J. Appl. Math. Comput. Mech. 23 (2024) 54-65. https://doi.org/10.17512/jamcm.2024.2.05.

[19] J. S. Abera, M.D. Firdi, E.H. Rikitu, J. Nanofluids. 13 (2024) 1096-1110. https://doi.org/10.1166/jon.2024.2192.

[20] M.M. Rahman, M.A. Rahman, M.A. Samad, M.S. Alam, Int. J. Thermophys. 30(2009) 1649-670. https://doi.org/10.1007/s10765-009-0656-5.

[21] K. Hsiao, Heat Mass Transf. 46 (2010) 413-419. https://doi.org/10.1007/s00231-010-0580-z.

[22] N.A. Yacob, A. Ishak, I. Pop, Comput. Fluids. 47 (2011), 16-21. https://doi.org/10.1016/j.compfluid.2011.01.040.

[23] K. Bhattacharyya, S. Mukhopadhyay, G.C. Layek, I. Pop, Int. J. Heat Mass Transf. 55(2012) 2945-2952. https://doi.org/10.1016/j.ijheatmasstransfer.2012.01.051.

[24] K. Bhattacharyya, Vajravelu, Commun. Nonlinear Sci. Numer. Simul.17(2012) 2728-2734. https://doi.org/10.1016/j.cnsns.2011.11.011.

[25] M. Hussain, M. Ashraf, S. Nadeem, M. Khan, J. Franklin Institute. 350 (2013) 194-210. https://doi.org/10.1016/j.jfranklin.2012.07.005.

[26] K. Singh, A. K. Pandey, M. Kumar, Heat Transfer Res. 50 (2019) 739-756. https://doi.org/10.1615/HeatTransRes.2018024647.

[27] B. Kumar, S. Srinivas, J. Appl. Comput. Mech. 6(2020) 259-270. https://jacm.scu.ac.ir/article_14580_81175fa2eddf2a1c75c8edac8f860396.pdf.

[28] R. Garg, J. Singh, U. S. Mahabaleshwar, O. Sayfidinov, G. Bognar, WSEASTrans. Fluid Mech. 18(2023) 24-33. https://doi.org/10.37394/232013.2023.18.3.

[29] M.S. Abel, P.S. Datti, N. Mahesha, Int. J. Heat Mass Transf. 52 (2009) 2902-2913. https://doi.org/10.1016/j.ijheatmasstransfer.2008.08.042.

[30] M.A.A. Mahmoud, S.E. Waheed, J. Egypt. Math. Soc. 20(2012) 20-27. https://doi.org/10.1016/j.joems.2011.12.009.

[31] H.T. Cheong, S. Sivasankaran, M. Bhuvaneswari, Int. J. Numer. Methods Heat Fluid Flow, 27(2017) 287-309. https://doi.org/10.1108/HFF-07-2015-0272.

[32] S.R. Mishra, Hoque, M. Mainul, B. Mohanty, N.N. Anika, Nonlinear Eng. 8 (2019) 65-73. https://doi.org/10.1515/nleng-2017-0126.
[33] M. Bhuvaneswari, S. Sivasankaran, A. Malarselvi, B. Ganga, Int. J. Energy Technol. Policy, 17(2021) 494-509. https://doi.org/10.1504/IJETP.2021.119863
[34] S. Sivasankaran, M. Bhuvaneswari, A.K. Alzahrani, Sci. Iran. 29(2022) 3063-3071. https://scientiairanica.sharif.edu/article_22932.html.
[35] H. Maaitah, O. Quran, N. Olimat, M. Duwairi, Int. Commun. Heat Mass Transf. 154(2024)107402. https://doi.org/10.1016/j.icheatmasstransfer.2024.107402.
[36] D.P. Palai, S. Chaudhuri, B. Das, J. Heat Mass Transf. Res. 12 (2025) 45-60. https://doi.org/10.22075/JHMTR.2024.32255.1496.

RADHAKRISHNAN MUTHUKRISHNAN[1]

PALANI GOVINDASAMY[2]

PARTHIBAN RAMACHANDRAN[3]

CHANDRASEKARAN EKAMBARAM[4]

[1]Department of Mathematics, Sri Venkateswara College of Engineering, Tamil Nadu, India
[2]Department of Mathematics, Dr.Ambedkar Govt. Arts College, Tamil Nadu, India
[3]Department of Mathematics, Nandanam Arts College, Chennai, India
[4]Department of Mathematics, Veltech Rangarajan Dr.Sagunthala R&D Institute of Science and Technology, Tamil Nadu, India

NAUČNI RAD

ANALIZA PRENOSA TOPLOTE PRI STRUJANJU MIKROPOLARNOG FLUIDA PREKO PROPUSNOG RAVNOG ZIDA KOJI SE ŠIRI ILI SKUPLJA

Ovo istraživanje razmatra strujanje mikropolarnog fluida u tački zastoja preko porozne ravne ploče koja se rasteže ili skuplja, uz uključivanje graničnih uslova klizanja brzine i temperature. Polazne parcijalne diferencijalne jednačine transformisane su u odgovarajuće obične diferencijalne jednačine primenom transformacija sličnosti, nakon čega su numerički rešavane primenom metode gađanja. Ispitan je uticaj glavnih fizičkih parametara na raspodele brzine, mikrorotacije i temperature, a rezultati su prikazani grafički. Pored toga, izračunate vrednosti koeficijenta naprezanja smicanja na zidu i brzine prenosa toplote za različite vrednosti parametara date su u tabelarnom obliku.

Ključne reči: granični sloj, prenos količine kretanja, metoda gađanja, klizanje brzine, zračenje, izvor/ponor toplote.